# Cortical Bone Vibrations Induced by Electromagnetic Field Pulse

Robert Royer, III[1], Walter Harders[1], Lee R. Moore[1], Caroline Androjna[1], Meredith Midura[1], Boris Kligman[1], Ronald J. Midura[1], Nianli Zhang[2], Erik I. Waldorff[2], James T. Ryaby[2], and Maciej Zborowski[1]

[1]Department of Biomedical Engineering, Lerner Research Institute, Cleveland Clinic, OH 44195 USA
[2]Orthofix Medical Inc., Lewisville, TX 75056 USA

**The purpose of our study was to test the hypothesis that the electromagnetic pulse (EMP) is capable of inducing mechanical vibrations in bone *ex vivo*. A thin segment of human femur diaphysis (from a tissue repository) suspended on a tensioned line (range $T = 2.2$–$123$ N) was exposed to EMP (mean $B = 0.64$ T, $dB/dt = 5877$ T/s, and the mean $B$-field gradient of 127 T/m) from a solenoid with axis orthogonal to tensioning line, forming a harmonic oscillator whose mechanical vibrations were measured using laser Doppler vibrometry (LDV, noise floor 1 $\mu$m/s). Calculated mean Maxwell stress and Lorentz forces acting on a weakly conducting, diamagnetic bone slice point away from the solenoid for maximum sensitivity of LDV measurement. The electromechanical origin of the LDV signal was confirmed by the order-of-magnitude agreement between calculated (range from 12 to 50 $\mu$m/s) and measured initial bone velocity amplitudes (e.g., 35.5 $\mu$m/s $\pm$ 7.5 $\mu$m/s at $T = 22.2$ N and 17.7 $\mu$m/s $\pm$ 2.5 $\mu$m/s at $T = 58.2$ N) and the increasing frequency (25–180 Hz) of decaying oscillations with the square root of $T$ over the range of line tensions ($r^2 = 0.978$, $p < 10^{-4}$, and $n = 17$). Theory and experiment show that magnetic field impulses are capable of exerting measurable mechanical forces on bone *ex vivo*. The results raise an interesting question if the electromechanical effect could be sufficiently large to contribute to bone remodeling, reportedly sensitive to vibration amplitudes as small as 1 nm, and considering long duration of orthopedic therapy using repetitive EMP (months).**

***Index Terms*— Biomagnetism, transcranial magnetic stimulation (TMS), very low-frequency electromagnetic field (VLFEM) and pulsed electromagnetic field (PEMF) stimulation.**

## I. Introduction

PULSED electromagnetic field (PEMF) is used in clinical therapy to minimize the need for surgical intervention and drug treatment. Low-frequency (1 kHz), low-field (1 mT) PEMF applied for few hours daily, over a period of three months, became an approved clinical modality in orthopedics for adjunct treatment to primary lumbar fusion surgery [1], [2]. High-field PEMF (over 1 T) includes transcranial magnetic stimulation (TMS) [3] and treatment of chronic depression [4].

Low fields used in the orthopedic PEMF applications do not reach the threshold of the neuronal activation (10 V/m) typical of TMS [5] and therefore are likely to interact with the bone biology by a different mechanism [6], [7]. A mechanism that has not been considered before is the potential contribution from the electromechanical forces, which could be important because of the living bone's high sensitivity to repeated, mechanical stimuli [8]–[10].

The purpose of this exploratory study was measurement of mechanical vibrations caused by magnetic field gradient impulses on bone *ex vivo*, as a preliminary step necessary toward biological investigations. The electromechanical PEMF effect may arise as a result of the interaction of imposed magnetic field with the induced electric current in bone (Lorentz force) and the bone magnetization discontinuity at the interface with the surrounding media (Maxwell stress). The experimental design specifically excluded confounding phenomena characteristic of vital tissue, such as response of peripheral nervous system neurons to electromagnetic pulse (EMP) by axonal depolarization [5], [11], [12].

A thin slice of human femur of known mass from a commercial tissue repository stored in electrolyte solution and pat dried with paper towel prior to the experiment was suspended on a stretched nylon string under controlled tension. This formed a mass-on-a-string harmonic oscillator whose vibrational frequency is tuned to the bone sample mass and the applied string tension and thus provides a sensitive detector element for the expected frequency response to EMP application [13]. To eliminate experimental artifacts, the vibrational frequency of the model was varied by varying the string tension. The thin slice of femur was positioned next to a short, thick solenoid powered by a short pulse of current from capacitors. The target area of bone was illuminated by a laser beam from a Doppler-effect vibrometer sensitive to bone surface velocity, theoretically predicted to be on the order of 10 $\mu$m/s, in the range of the expected bone sample oscillation frequency (100 Hz).

## II. Materials and Methods

### A. Theory

The magnitude of the electromechanical force density on bone suspended on a stretched string was calculated from equations of classical electrodynamics for a limiting case of extremely low-frequency oscillating magnetic field (no radiative component). In general, the pulsed magnetic field exerts a mechanical force on electrically conductive and magnetically susceptible media [14], [15]. For the special case of linear,

Manuscript received October 29, 2021; revised February 17, 2022; accepted March 22, 2022. Date of publication April 27, 2022; date of current version June 29, 2022. *(Robert Royer, III and Walter Harders contributed equally to this work.)* Corresponding author: M. Zborowski (e-mail: zborowm@ccf.org).

This article has supplementary downloadable material available at https://doi.org/10.1109/TMAG.2022.3169083, provided by the authors.

Digital Object Identifier 10.1109/TMAG.2022.3169083

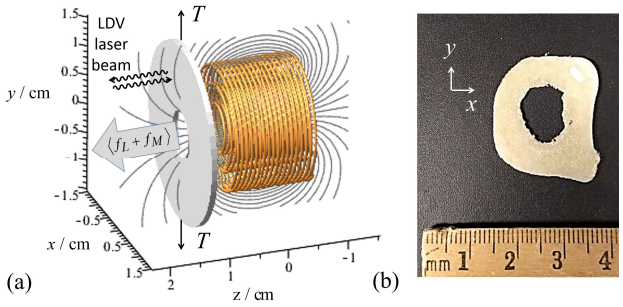


Fig. 1. EMP solenoid and the bone sample. (a) Solenoid and bone slice model showing divergent $B$-field lines at the location of the bone sample; laser light imping on and reflected off the bone sample; the suspending line tensioned with force $T$; and the direction of the EMP force from the contributions of Maxwell stress and Lorentz body force contributions averaged of the bone slice volume, $\langle f_L + f_M \rangle$. (b) Photograph (axial view) of the human femur slice, thickness 1 mm along the $z$-axis.

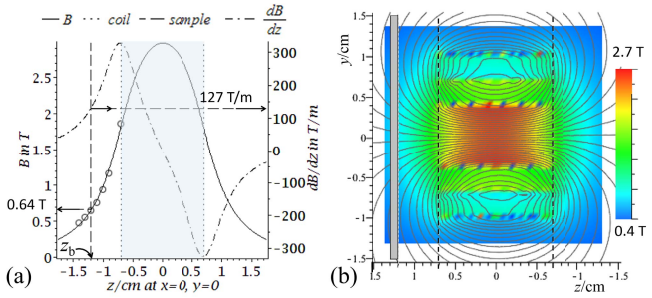


Fig. 2. $B$-field and its $z$-gradient along the EMP coil axis. (a) Shaded area indicates coil axial extension. The theoretical model values are indicated by lines, and the measured values are indicated by open circles. Arrows indicate local $B$-field and $z$-gradient values at a point of intersection with the bone slice plane where the $dB/dt$ values were measured. (b) Corresponding false-color $B$-field map at the axial plane of the coil. The light gray rectangle outline indicates the location of bone slice of thickness $d$.

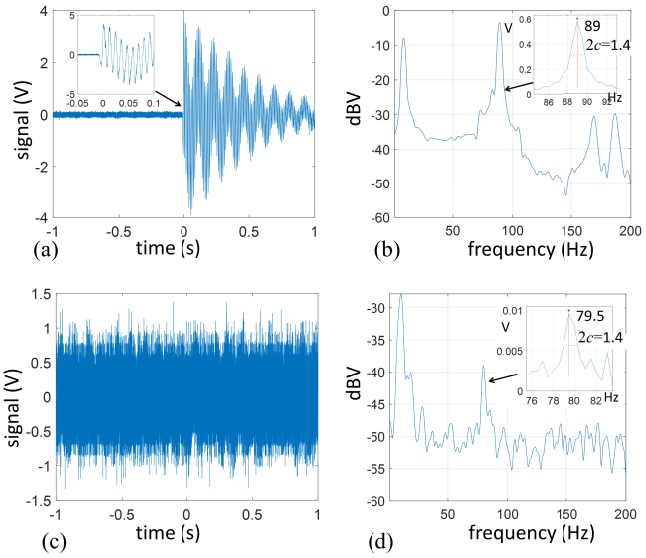


Fig. 3. Time- and frequency-domain signals acquired by LDV in 2 s time window before and after application of (a) and (b) mechanical control and (c) and (d) test electromagnetic (EM) pulse for low string tension of 22.2 N. Both types of pulses cause bone sample vibrations in low- and high-frequency ranges (especially near 10 and 80 Hz). The higher frequency is at resonance calculated for the tensioned string oscillator. The non-resonant frequency components seen in the spectrum of a strong mechanical pulse (a) are related to the additional bone target degrees of freedom not accounted for by the simple model of the tensioned string resonator.

weakly conducting and weakly magnetic media, characteristic of bone, there are two types of electromechanical forces to consider: the Lorentz body force due to the induced, local current interaction with the imposed, oscillating magnetic field and Maxwell stress force on bone mineral and interstitial fluid due to their differential magnetic susceptibilities. The analysis of those two types of forces provides rationale for the experimental study, as described next. We have developed an analytical model to calculate the magnetic field and electromechanical force distributions over the surface of a thin bone slice suspended on a thin, tensioned string next to the solenoid, as shown in Fig. 1 and further described in Supplementary Information and illustrated in Supplementary Figs. 1–4. The model input and output parameters are listed in the Appendix, in Tables I and II, respectively.

The kinetics of the bone vibrational response to EMP was modeled by a damped harmonic oscillator forced for short duration, $\Delta t \ll {}^1\!/_2(2\pi/\omega_0)$ impulse, $\langle f \rangle = \langle f_L + f_M \rangle$ (sum of Lorentz and Maxwell stress body forces) approximated by the Dirac delta function, $(\langle f \rangle/\rho)\delta(t/\Delta t)$. The solution for vibration velocity in the case of weakly damped oscillator and initial conditions $x_{0-} \equiv x(t < 0) = 0$ and $v_{0-} \equiv dx/dt(t < 0) = 0$ is a decaying sinusoid

$$v = \frac{\langle f \rangle}{\rho} \Delta t\, e^{-ct} \frac{\cos\left(\sqrt{\omega_0^2 - c^2}\, t\right)}{\sqrt{\omega_0^2 - c^2}}, \quad t \geq 0, \ \omega_0 = \sqrt{\frac{T}{m_0 L}} \tag{1}$$

where $\rho$ is the bone density, $c$ is the damping constant, $\omega_0$ is the natural angular frequency of the harmonic oscillator, $m_0$ is the bone sample mass, $T$ is the line tension of length $L$, and the pointed brackets $\langle \ldots \rangle$ denote average over the bone sample volume. For representative experimental values of $T = 1$ kg $= 9.81$ N, $L = 10$ cm, and $m_0 = 1$ g, one obtains $\omega_0 = 2\pi \times 70.5$ Hz, corresponding to a period of 14 ms, which is much longer than the applied EMP duration of 0.334 ms, thus justifying the EMP approximation by Dirac delta in the model. Further details are provided in the Supplementary Information.

The initial velocity in response to EMP is obtained by taking the right-handed limit at $t = 0$

$$v_{0+} = \lim_{t \to 0+} v(t) = \frac{\langle f \rangle}{\rho} \Delta t. \tag{2}$$

The magnitude of $v = v(t)$ spectral distribution $|\tilde{v}| = |\tilde{v}(\omega)|$ is calculated by its Fourier transform

$$|\tilde{v}| = \frac{\langle f \rangle}{\rho} \Delta t \sqrt{\frac{2}{\pi}} \frac{\omega}{\sqrt{\left(\omega_0^2 - \omega^2\right)^2 + (2\omega c)^2}}$$
$$\xrightarrow{\omega \to \omega_0} \frac{1}{\sqrt{2\pi}} \frac{\langle f \rangle}{\rho} \frac{\Delta t}{c} = \frac{v_{0+}}{\sqrt{2\pi}\, c}. \tag{3}$$

The last equation on the right results from substitution of (2) into (3). The damping coefficient $c$ was estimated from

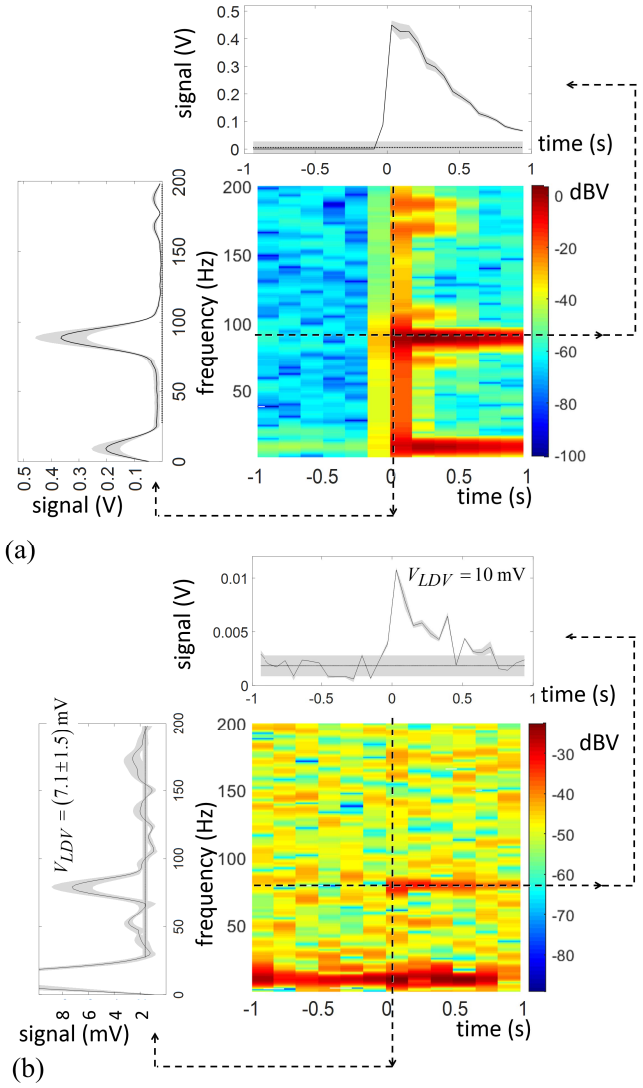


Fig. 4. Spectrograms and marginal plots of bone sample responses to (a) mechanical and (b) EMP stimulation for low resonator string tension of 22.2 N. The spectrograms show resonator vibration onset at the time of the impulse application [mechanical in (a) and EMP in (b)]. The top marginal plots show ±2 Hz bandpass signal centered at the resonator frequency showing the presence of weak EMP signal (b) buried in the raw broadband (20 kHz) signal [Fig. 3(c)]. The side marginal plots show frequency spectra for a short time window ±50 ms centered at 125 ms after impulse application for better signal isolation from noise. Gray bands indicate noise floor calculated as an error of the median value (prior to the impulse application for time sequence histograms, top, and for frequencies >30 Hz for frequency sequence histograms, side). Small differences in EMP peak $V_{\mathrm{EMP}}$ values between time and frequency histograms are the result of finite time and frequency resolutions of the LDV measurements. Note evidence of low-frequency (10 Hz) vibration before impulse application [mechanical in (a) and EMP in (b)] indicating its extraneous origin (environmental noise).

the experimental resonance peak width of the laser Doppler vibrometry (LDV) frequency spectra, considering that the resonance peak's full-width at half-maximum is FWHM $\approx 2c$ [see insets in Figs. 3(b) and 5(b)] and the low signal-to-noise ratio of the EMP peak [Figs. 4(b) and 6(b)]. The analytical Fourier transform coefficients in (3) (in the units of distance, meters) differ from the discrete Fourier transform (DFT) coefficients (in the units of velocity, m/s) calculated from the LDV time sequences by the DFT bandwidth resolution factor

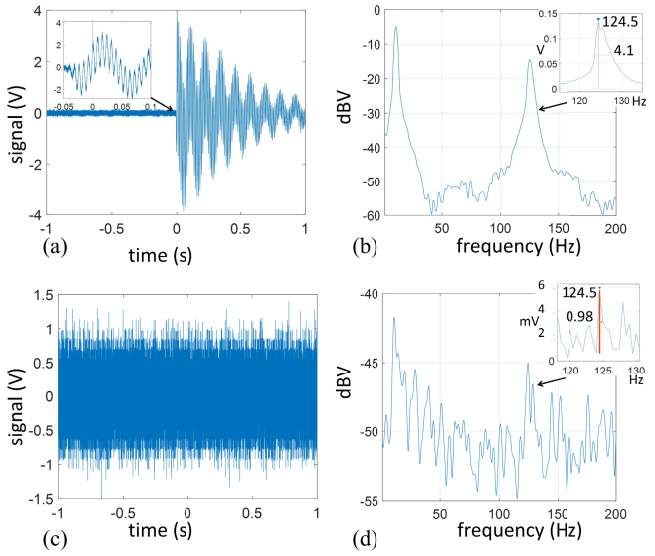


Fig. 5. For comparison with Fig. 3, at high resonator string tension of 58.2 N. (a) and (b) Results of mechanical control. (c) and (d) Results of test EMP. Note shift in the resonator frequency from 80 to 125 Hz compared to corresponding panels in Fig. 3, as expected from the tensioned string oscillator model. Note the absence of such a shift for the low-frequency peak (10 Hz), indicating its origin being unrelated to the force impulse application.

(here equal to 0.5 Hz). For comparison of calculated $V_{\mathrm{EMP}}$ with the measured $V_{\mathrm{LDV}}$ peak heights, we used a product of the DFT bandwidth resolution (0.5 Hz) and the LDV instrument constant of (200 V)/(m/s), Table I, as a conversion factor

$$V_{\mathrm{EMP}} = 200\left[\frac{\mathrm{V}}{\mathrm{m/s}}\right] \times [0.5\ \mathrm{Hz}] \times \frac{v_{0+}}{\sqrt{2\pi}\,c}[\mathrm{m}] = 100\frac{v_{0+}}{\sqrt{2\pi}\,c}[\mathrm{V}]. \tag{4}$$

The theoretical values $V_{\mathrm{EMP}}$ are shown in Table II, and experimental ones $V_{\mathrm{LDV}}$ were read from the LDV spectra [such as shown in Figs. 4(b) and 6(b)].

In summary, the presence of $V_{\mathrm{LDV}}$ peak in the LDV frequency spectra at the natural frequency (eigenfrequency) of the oscillator, $\omega = \omega_0$ following EMP application; its frequency dependence on the string tension $T$ as predicted from the resonance frequency of the oscillator; and its height, $V_{\mathrm{LDV}}$ being of the same order of magnitude as that predicted from the theoretical model, $V_{\mathrm{EMP}}$, completes the proof of electromechanical effect of EMP impulse on bone.

### *B. Experiment*

*1) Bone Sample:* A sample of human femur diaphysis was used for this research. The specimen was from cadaver donor. It was acquired through accredited specimen suppliers (Science Care, Inc., and Anatomy Gifts Registry), who consented donors for the use of donated tissue for education and training, scientific advancement, and/or research and development purposes. According to the U.S. federal regulations (45 Code of Federal Regulations Part 46) and the Cleveland Clinic Institutional Review Board (IRB) guidelines, the study did not qualify as research involving human subjects. No individually identifiable health information about the donor was disseminated. Demographic information is provided to support

research utility of the specimen. The donor does not belong to any rare identifiable group.

The femur diaphysis was cut along the transverse plane into 1 mm-thick slices. The resulting annular slices of cortical bone were stored at 4 °C in a phosphate-buffered saline (1× PBS) and 0.1% sodium azide ($NaN_3$) solution when not in use. When being used, the samples were removed from the storage solution and tapped dry with a paper towel, but considered "wet" because of presence of electrolyte solution bound in the bone structure. The mass of the bone slice used for this series of experiments was 0.897 g that was typical of the mass of all bone slice preparations available for this study, ($0.841 \pm 0.327$) g, $n = 4$.

*2) Apparatus:* A bone sample was suspended via a single point on nylon thread, itself supported in a custom-made wooden housing with adjustable "frets" allowing for variation in string length and tension. Monofilament nylon-blend polymer thread (Trilene, 22.7 kG test, 0.71 mm diameter) was used to suspend the sample at the midpoint of the frets and attached using a minimal amount of reusable caulking cord. The tension was achieved by attaching masses to the lower end of the thread. The structure was then bolted to a Newport pneumatic vibration isolation table to mitigate exterior mechanical vibrations from affecting the bone sample (Supplementary Fig. 1). To further avoid unwanted mechanical vibrations from the coil directly affecting the bone motion, the coil was affixed to a separate tripod (Manfrotto 475b). A 2-D translation stage (Newport, 462-XY-M) mounted on the tripod allowed precise positioning of the coil relative to the bone. The potential other sources of the mechanical impulse transfer from coil to the bone sample above the LDV sensitivity threshold were ruled out by the relatively large masses and the resulting large inertia of the system components compared to that of the bone oscillator, their physical separation, and additional testing for possible sound and heat transfer artifacts (results not shown).

*3) Electromagnetic Pulse:* The bone sample was subjected to an EMP from a solenoid (1.15 mm diameter copper wire, six layers, 60 turns, 39.0 mΩ, 22.04 $\mu$H, OD: 2.18 cm, ID: 0.79 cm, and $L$: 1.27 cm) with current supplied by a capacitor. The coil, internally referenced as "17–6," had a geometric factor $G = 0.178$, where 0.179 is considered to be ideal to maximize the field strength $H$ per watt of real power dissipated in the windings.

*4) Capacitor Discharge Circuit:* A capacitor discharge circuit (CDC) was developed in-house to provide the EMP. It comprises: 1) charging circuit based on a variable transformer and a voltage doubler that also provides rectification to dc; 2) low equivalent series resistance, metallized polypropylene film capacitor (470 $\mu$F, $1000V_{\max}$); and 3) discharge circuit based on an SCR thyristor and an emitter follower allowing a buffered connection to an external triggering device, such as an arbitrary waveform generator or microcontroller (Arduino Uno). The thyristor could also be manually fired by a 1.5 V, 150 mA gate-to-cathode pulse given by a 6 V switched-mode power supply and toggle switch.

Low noise, 120 V, 60 Hz, alternating current (ac) was supplied to the circuit and test equipment via uninterruptible power supply (Tripp-lite SU1500XL). The ac voltage to the capacitor was controlled with a 10 A variable transformer and then stepped up and rectified by a voltage doubler circuit that provided 0–360 VDC. A 40 Ω wirewound control resistor allowed a charge time of 100 ms for repeat discharge rate up to 10 Hz. When discharging the capacitor at 300 V through coil 17–6, the current peaked at 1122 A at 146 $\mu$s. Theoretical prediction gave us the current slew rate maximum of $1.37 \times 10^7$ A/s, occurring instantaneously after triggering. Current flowed during a half period of oscillation of 334 $\mu$s, at which time it was shut off by an instantaneous reversal in current through the thyristor, a type of solid-state switch that only allows current to flow in one direction [Supplementary Fig. 2(c)]. The capacitor voltage was monitored by a benchtop digital multimeter (DMM) (Keysight U3402A). Due to its high voltage and current capabilities, safe operation of the CDC was ensured by proper grounding, physical isolation, and careful operation. The apparatus was encased within a wooden box and electrically shielded and grounded by covering the exterior of the box with conductive foil tape (3M 3340 aluminum foil 4 mil = 102 $\mu$m thick). The supply leads to the coil were 2.2 mm diameter Cardas Litz wire with Teflon insulation and were twisted together and covered with copper braid shield, connected to Earth ground.

*5) Laser Doppler Vibrometry:* The LPO1 (OMS Corporation, Laguna Hills, CA, USA) laser Doppler vibrometer was connected to an optional Digital Signal Demodulator (DSD, National Instruments PXIe-1071) that improves the sensitivity 4–5 fold compared to the digital-to-analog converter internal to the LP01, resulting in the nominal noise floor not higher than 1 $\mu$m/s. The DSD 10.7 MHz FM output bypasses the internal analog decoder of the LP01. The analog output of the DSD was fed to the oscilloscope. The bone velocity was measured by the Doppler frequency shift in the low range bandwidth setting such that 1 V corresponded to 5 mm/s. The head unit employed a custom-built lens that reduced beam diameter from 1 to 0.1 mm and had a focal length of approximately 15 cm. The collimated, near-infrared beam (wavelength 780 nm) was aimed at the bone slice at an approximately right angle to its surface [Fig. 1(a) and Supplementary Fig. 1]. The velocity of the bone sample was visualized and recorded by an Agilent 2000 series oscilloscope.

The oscilloscope samples the voltage from the LDV at 50 ksamples/s over a 2 s window and outputs 100 000 measurements at 20 $\mu$s time resolution. The EMP triggers this acquisition window by way of a small search coil ($1.05 \times 10^{-3}$ turns-m$^2$) placed next to the EMP coil, whose output is sent to a second channel of the oscilloscope. This ensured synchronicity of the effect of the pulse on the bone and the acquisition.

*6) Data Acquisition and Processing:* The experimental testbed was optimized using MATLAB R2018a software with Instrument Control and Signal Processing Toolboxes to expedite data acquisition. By using the Standard Commands for Programmable Instruments (SCPI) commands, both the

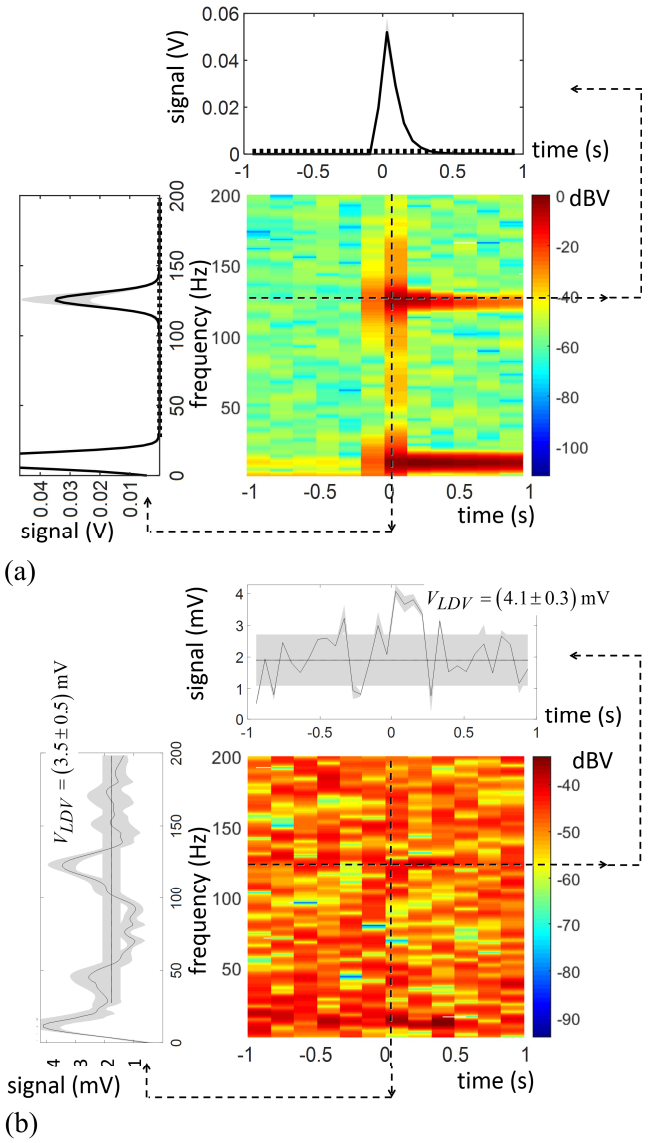


Fig. 6. For comparison with Fig. 4, at high resonator string tension of 58.2 N. The spectrograms show resonator vibration onset at the time of the impulse application [mechanical in (a) and EMP in (b)]. The vibrational EMP effect in panel (b) is comparatively weak as expected of a weaker response of a tensioned string oscillator, but still detectable and shifted toward higher frequencies as expected. As in Fig. 4, small differences in EMP peak $V_{\mathrm{EMP}}$ values between time and frequency histograms are the result of finite time and frequency resolutions of the LDV measurements.

digital oscilloscope and Arduino Uno were controlled through a MATLAB interface, allowing acquisition of oscilloscope output voltage time sequences (each 100 000 long) with the push of a button.

Data analysis and processing was completed using MATLAB R2018a, as well as its Signal Processing Toolbox. The recorded oscilloscope voltage time sequences were averaged point by point over ten repeated acquisitions. The frequency analysis was done by running MATLAB DFT on the averaged time sequences. The MATLAB DFT routine outputs the LDV voltage spectrum frequency sequence at 1.0 Hz resolution and the length of 25 000 corresponding to 25 kHz bandwidth (single-sided, below Nyquist limit), in volts (the same units as the input time sequence). Results were displayed as: 1) time and frequency plots; 2) frequency versus time power density spectrograms (in decibel volt and linear scales); and 3) as spectrograms for a narrow frequency band around the eigenfrequency of the oscillator and a short-time window coinciding with the time of EMP application. Peaks in the EMP test signal frequency spectrum were visually inspected and compared to the mechanical control signal (Figs. 4–7). The EMP and the mechanical control peak frequencies $\omega_0$ were plotted against the line tension $T$ and visually compared with the expected values from the bone oscillator model (1) by plotting them against a range of the eigenfrequencies at varying oscillator string lengths, $L/2$ to $L$, to account for imperfections of the simple harmonic oscillator model. The mechanical and EMP peak frequencies were compared by plotting them one against the other and tested for identity by a linear regression analysis.

## III. Results

The experiment tested theoretical predictions of a significant mechanical effect of EMP on weakly conducting, diamagnetic bone slice, in experimental settings as shown in Fig. 1 and Supplementary Fig. 1, for parameters listed in Tables I and II. The relative placement of the EMP solenoid and the LDV detector around the bone slice sample suspended on the tensioned string forming an oscillator maximized the LDV signal by constraining bone vibrations to the direction of the LDV laser beam propagation [Supplementary Fig. 3(e)–(f)].

The calculated spatial $B$-field variation was validated by measuring the rate of change amplitude of a magnetic field ($dB/dt$) with a search coil placed at the bone slice location (5 mm on-axis away from the EMP solenoid, see Fig. 2) and connected to a digital oscilloscope. The shape of $dB/dt$ measured at the bone sample position [Supplementary Fig. 2(c)] corresponded closely to the $dB/dt$ function of time calculated for the CDC parameters [CDC, compare to Supplementary Fig. 2(b) and (c)].

Fitting the $B$-field mathematical model, Supplementary (5) to experimental $dB/dt$ values [Fig. 2(a)] fixed the only free parameter of the $B$-field model, the coil current $I$ that is subsequently used to calculate the EMP forces acting on the bone slice [Supplementary (8) and (10)], which are then used to calculate the vibration velocity (1) and, in the end, the initial velocity amplitude following EMP application (3). The control over the $dB/dt$ impulse was achieved by controlling voltage of the CDC charging circuit and was key to the system's capability of delivering accurate peak $dB/dt$ levels. Another important aspect of the CDC design was that it suppressed coil current "ringing" after the initial current pulse [Supplementary Fig. 2(c)] and, thus, limited the EMP duration to a narrow window of time ($\Delta t \approx 334\ \mu$s) that was much shorter than the bone oscillation period ($\Delta t \approx$ 5–40 ms, shown in Figs. 3–6). This justified the EMP impulse approximation by a Dirac delta in the forced harmonic oscillator model (1).

The LDV instrument constant of 1 V $\equiv$ 5 mm/s was used to calculate the theoretically expected LDV signal height in volts, $V_{\mathrm{EMP}}$, from the bone oscillator Fourier transform peak height (4), for comparison with the experimentally measured LDV

spectral peak height, $V_{\mathrm{LDV}}$ [in volts, in Figs. 4(b) and 6(b)]. Mechanical vibration spectra (arising from a direct strike of the string by a wooden object) were used to confirm the expected location of the EMP vibrational peak.

The vibrational signal in response to EMP application is clearly discernible in the LDV spectra shown in Figs. 3–6 at frequencies corresponding to the resonance frequency of the bone mass oscillator model (1). The EMP spectral peak locations correspond to those of the mechanical impulse controls and vary with the string tension $T$ in the same manner as their mechanical counterparts, thus eliminating the possibility of an artifact of the EMP interaction with the electronics of the measuring apparatus.

The measured EMP spectral peak heights $V_{\mathrm{LDV}}$ of a few millivolts were much smaller than those seen in the mechanical control spectra measured in volts (Figs. 3–6), as expected of a weak interaction of EMP with the bone sample. Notably, the calculated EMP peak height values for the Maxwell stress model $V_{\mathrm{EMP}}$ from (3) and (4) and Supplementary (10) shown in Table II were within the range of those read from the experimental LDV frequency histograms [$V_{LDV}$, Figs. 4(b) and 6(b) marginal histograms]. The difference between the two (on the order of 1 mV) is attributed to the number of simplifying assumptions used in the theoretical model and the uncertainties in the exact experimental parameter values (such as bone slice axial distance from the solenoid).

The $V_{\mathrm{EMP}}$ sensitivity to input parameter perturbations was estimated by repeating the calculations at two extremes of the bone slice axial position, $z_b = (12 \pm 2)$ mm (Table I) accounting grossly for uncertainties in the exact bone slice distance from the coil center, deviation of femur slice geometry from a perfect annular disk, and the non-ideal coil winding. As expected, $V_{\mathrm{EMP}}$ rise was faster (from 2.3 to 5.0 mV) with the decreasing distance to coil than its fall (from 2.3 to 1.2 mV) with the increasing distance from the coil (Table II). The corresponding initial bone velocities calculated from the Maxwell stress model (3) and Supplementary (10), shown in Table II, were low; 23 $\mu$m/s and the limits of [12, 50 $\mu$m/s] but well above the noise level of the LDV detector (1 $\mu$m/s). The range of calculated $V_{\mathrm{EMP}} \in [1.2,\ 5.0]$ mV was near the range of the experimental LDV range $V_{\mathrm{LDV}} = 7.1\ (\pm 1.5)$ mV [Fig. 4(b)] or overlapped with it $V_{\mathrm{LDV}} = 3.5\ (\pm 0.5)$ mV [Fig. 6(b)], which confirmed the model predictions. The corresponding values of the experimental, initial bone velocity were 35.5 ($\pm$7.5) $\mu$m/s and 17.5 ($\pm$2.5) $\mu$m/s considering the instrument constant of 5 mm/s/V. The initial bone velocities calculated from the Lorentz force model Supplementary (3) and (8), shown in Table II, were lower by over four orders of magnitude, indicating that the Maxwell stress effect predominates under the selected experimental conditions and is the only significant contribution to the experimentally measured LDV signal.

The low-frequency peak at $f = 10$–$30$ Hz appearing in both EMP test and mechanical control spectra did not depend on string tension and was occasionally detectable prior to EMP [Fig. 4(b)] or mechanical stimulation application [Fig. 6(a)] and therefore was an artifact likely related to mechanical resonance of the bone oscillator support frame generated by the random noise of the laboratory environment (insufficient isolation from the building's heating, ventilation, and air conditioning system). The occasional frequency peaks not apparently related to string tension suggested the presence of additional degrees of freedom of bone vibrations due to departure of the experimental setup from ideality such as irregular shape of the bone slice [Fig. 1(b)] and the point suspension of the bone sample allowing possible angular motion (Fig. 1 and Supplementary Fig. 1).

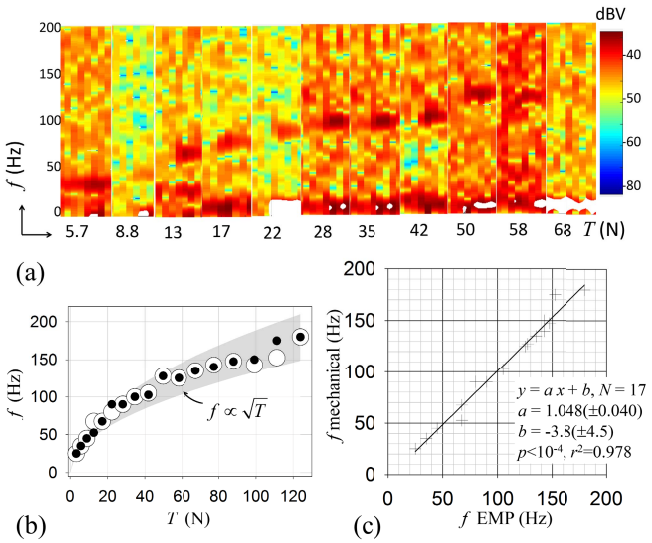


Fig. 7. Vibrational frequency of the suspended bone sample after EMP application as a function of the line tension $T$ and comparison with the mechanical control. (a) Montage of selected set of EMP spectrograms 0.5 s before-to-after EMP application showing increase of eigenfrequency $f_0$ with the increasing string tension $T$. (b) Plot of full set of resonator frequencies $f_0$ against the string tension $T$ after mechanical (full circles) and EMP (open circles) impulse application, against a gray band of resonator frequencies calculated between the limits of full- and half-length of the resonator string, indicating agreement with the square root dependence on string tension. (c) Same data plotted as mechanically induced frequency against the EMP induced frequency showing excellent agreement between the two (regression line nearly overlapping the identity line) and thus providing proof of EMP electromechanical (vibrational) effect on bone. The data were collected at $dB/dt = 5877$ T/s.

When plotted as a function of string tension, the characteristic LDV peak frequencies were increasing with the increasing string tension [Fig. 7(a)] in agreement with the square root dependence on tension $T$ in (1) and Fig. 7(b). The EMP-triggered signal vibrational frequency dependence on string tension coincided with that of the mechanical control [Fig. 7(c)] providing further support for the mechanical effect of EMP on the bone model. The agreement between the EMP-induced and mechanically induced bone vibration frequencies was exact to be within the experimental error [regression line slope of 1.048 $\pm$ 0.040, $p < 10^{-4}$, close to the identity, see Fig. 7(c)].

## IV. Discussion

The study was designed to answer the question if a single EMP is capable of exerting a mechanical force on cortical bone, discoverable in principle by measuring change of its momentum using a highly sensitive mechanical oscillator and LDV system. The underlying motivation was our long-standing interest in understanding the biophysical mechanisms

of action of low-frequency, low magnitude PEMFs approved for selected orthopedic therapies [16]–[18]. Theoretical treatment of the problem based on the bulk material properties of the cortical bone sample and the parameters of the experimental system revealed that the Maxwell stress force, but not the Lorentz force, is sufficiently large to rise above the noise floor of the LDV detector.

The *ex vivo* experiments performed on devitalized, wet-stored, cortical bone sample eliminated the possibility of axonal polarization as a potential confounding factor in interpretation of data in the context of their potential biological significance.

The detection of weak vibrational signal was made possible by unique features of the experimental system that minimized mechanical noise of the bone suspension apparatus and laboratory environment, and the potential electrical noise from EMP interaction with the electronic equipment. The ability to search for the weak signal in a narrow frequency band known *a priori* from the natural frequency of the mechanical oscillator, and to vary the oscillator eigenfrequency in order to test the conjecture of the signal's mechanical origin, was critical for establishing experimentally the electromechanical, vibrational effect of EMP.

The effect of bone magnetization was noted by others before, in various experimental conditions. The mean bone mineral volume magnetic susceptibility of $-1.12 \times 10^{-5}$ is low but not negligible, its magnitude being approximately 20% greater than that of water, $-9.05 \times 10^{-6}$ and detectable by the MRI [19]. The magnetization anisotropy of the major bone mineral component, hydroxyapatite, is sufficiently large for the Maxwell stress to cause mechanical alignment of its polycrystalline component with the strong magnetic field vector, used for structural analysis [20]. The Lorentz force arising from interaction of the (induced) electric current in tissue and the combination of imposed oscillating and strong, and constant $B$-fields are capable of imparting mechanical force on tissue under carefully controlled laboratory conditions [21]–[23] and were also considered as a contributing factor in TMS biological effects [24]. We have previously reported on mechanical effect of slowly oscillating magnetic field (1 Hz) on bulk bone [25].

For the study reported here, the maximal rate of $B$-field changes with time, and $dB/dt$ (the "slew rate" [26]) was approximately an order of magnitude higher than that shown by others to be effective for bone regeneration *in vivo*, 5877 T/s compared to up to 500 T/s [16], [27]. Considering that the Maxwell stress force is a quadratic function of the $dB/dt$ slew rate, Supplementary (5) and (10), it follows that for an equal rise time to peak value, the slew rate of 300–500 T/s PEMF used in previous *in vivo* animal studies [16], [27] would have 200–100-fold smaller vibrational effect ($\sim$0.2 $\mu$m/s) than the $\sim$6000 T/s EMP used in current *ex vivo* experiments ($v_M =$ 23 $\mu$m/s, Table II). Also, the Maxwell stresses inside living bone are likely to be lower than those calculated for the present study because of a smaller difference in magnetic susceptibility between the bone mineral and the interstitial fluid ($\Delta\chi = \sim 1 \times 10^{-6}$) than the bone mineral and the air ($\Delta\chi = \sim 1 \times 10^{-5}$) characteristic of this study. Nevertheless, mechanical vibrations in the nanometer-to-submicrometer range have been reported to have a biological effect on bone when applied over an extended period of time [10].

Considering a complex bone architecture, a large interfacial surface area between bone mineral and the interstitial fluid compartment, and the interconnectedness of bone cellular network, the cumulative effect on bone metabolism of PEMF mechanical force could be significant, analogous to the mechanical effect of low-energy therapeutic ultrasound reported to augment spinal fusion [28], [29].

The living bone is in an active state of homeostasis resulting in an exquisite sensitivity to mechanical cues that determine its structure and regeneration rate [8], [9], [16]. We speculate that it is therefore plausible that even weak mechanical vibrations caused by prolonged PEMF application for as long as a few months, prescribed by current PEMF clinical treatments, could result in altered bone remodeling and contribute to the therapeutic effect.

The chronic, long-term effects of moderate PEMF have been documented to improve the management of selected orthopedic conditions refractory to standard treatment [30]–[32], yet its mechanism of action is not fully understood as it may depend on many different pathways [33]. Our experiment suggests that PEMF electromechanical stimulus could be sufficiently large to be considered as a factor in activating regulatory pathways that respond to mechanical bone stimulation and a worthy subject for future studies.

## V. Conclusion

PEMF is used in orthopedic therapy [16], [34], [35], but there is no established mechanism of its action *in vivo* notwithstanding its known *in vitro* effects related to induced currents on calcium ion ($Ca^{2+}$) transport and the molecular signaling [6], [7], [36], [37] important for bone homeostasis. The results of this study suggest the importance of assessing molecular markers of bone cell responses to mechanical stimuli in future studies on the PEMF mechanism of action on bone remodeling. They also suggest that the *in vitro* results from 2-D cell cultures may not be directly translatable to the *in vivo* and clinical situations because of the lack of 3-D mineral structure in 2-D cell cultures. These conclusions echo earlier observations by others of the importance of ordered structures, of much larger dimensions than a single cell, for an efficient absorption of PEMF energy for it to be important for bone regeneration [38]–[40].

## Appendix

See Tables I and II.

## Acknowledgment

This work was supported by the Sponsored Research Agreement between Cleveland Clinic and Orthofix Medical Inc., Lewisville, TX, USA, under Grant ORTHF1606MZ.

Application of laser Doppler vibrometry to detection of small bone vibration was suggested by Dr. Aaron Fleischman.

TABLE I
MODEL INPUT PARAMETERS

| Part | Symbol | Value | Units | Description |
|---|---|---|---|---|
| Bone | $\Delta\chi$ | $-1.0\times10^{-5}$ | | Bone-air mag. susceptibility |
| | $\sigma$ | 0.01 | S/m | Conductivity |
| | $d$ | 1.0 | mm | Bone thickness |
| | $r_o$ , $r_i$ | 1.5, 0.4 | mm | Bone outer, inner radii |
| | $V$ | 0.657 | $cm^3$ | $\pi\left(r_o^2 - r_i^2\right)d$ |
| | $m_0$ | 0.897 | g | Bone slice mass |
| | $\rho$ | 1,365 | $kg/m^3$ | $m_0/V$ bone density |
| | $z_b$ | 12.0±2.0 | mm | Distance to coil center |
| | $\langle B\rangle$ | 0.22(±0.18) | T | Mean±SD on bone surface |
| | $\langle E\rangle$ | 3.7(±2.5) | V/m | Mean±SD on bone surface |
| Coil | $R_i$, $R_c$, $R_o$ | 4.0, 7.125, 10.25 | mm | Inner, mid, and outer radii |
| | $N$ | 18 | | Turns per spiral layer |
| | $N_i$ | 8 | | Line segments per turn |
| | $L$ | 14.0 | mm | Length of solenoid |
| Oscillator | $c$ | 0.5 – 0.75 | Hz | Damping coeff. |
| EMP | $\Delta t$ | 0.334 | ms | Pulse duration |
| | $\mu_0$ | $4\pi\times10^{-7}$ | T.m/A | Free space permeability |
| | $B_0$ | 0.64 | T | Max. B on bone surface |
| | $dB/dz$ | 127 | T/m | Max. B grad on bone surface |
| | $dB/dt$ | 5,877 | T/s | Max. dB/dt on bone surface |
| LDV | *constant* | 5 | (mm/s)/V | LDV Instrument constant |

TABLE II
MODEL OUTPUT PARAMETERS

| Part | Symbol | Value | Units | Ref. | Description |
|---|---|---|---|---|---|
| Coil | $\langle dI/dt\rangle$ | $2.6\times10^6$ | A/s | Suppl. Fig. 2 | RMS current rate of change over EMP duration |
| | $\langle I\rangle$ | 840 | A | Suppl. Fig. 2 | RMS current over EMP duration |
| | $\langle j\rangle$ | 37(±25) | $mA/m^2$ | Suppl. Fig.4(a) | Mean (on bone cross-section) induced current density |
| | $\langle f_L\rangle$ | 6.4(±4.6) | $mN/m^3$ | Equation (S8), Suppl. Fig.4(b) | Mean (on bone cross-section) Lorentz body force |
| | $v_L = v_{0+}$ | 0.002 | μm/s | Equations (2), (S8) | Initial velocity imparted by induced Lorentz force |
| | $V_{EMP}$ | 0.4 | μV | Equations (4), (S8) | LDV spectral EMP peak (theory, Lorentz) |
| | $\langle f_M\rangle$ | 100(±130) | $N/m^3$ | Equation (10), Suppl. Fig.4(d) | Mean (on bone cross-section) Maxwell body force |
| | $v_M = v_{0+}$ | 23 | μm/s | Equations (2), (S10) | Initial velocity imparted by Maxwell stress force |
| | $V_{EMP}$ | 2.3 | mV | Equations (4), (S10) | LDV spectral EMP peak (theory, Maxwell) |
| | $V_{EMP}{}^+$ | 5.0 | mV | Equations (4), (S10) | $V_{EMP}$ over-estimate at $z_b$ – 2 mm |
| | $V_{EMP}{}^-$ | 1.2 | mV | Equations (4), (S10) | $V_{EMP}$ under-estimate at $z_b$ + 2 mm |

## REFERENCES


[1] C. T. Rubin, K. J. McLeod, and L. E. Lanyon, "Prevention of osteoporosis by pulsed electromagnetic fields," *J. Bone Joint Surg. Amer.*, vol. 71, pp. 411–417, Mar. 1989.

[2] E. I. Waldorff, N. Zhang, and J. T. Ryaby, "Pulsed electromagnetic field applications: A corporate perspective," *J. Orthopaedic Transl.*, vol. 9, pp. 60–68, Apr. 2017.

[3] V. Walsh and A. Cowey, "Transcranial magnetic stimulation and cognitive neuroscience," *Nature Rev. Neurosci.*, vol. 1, pp. 73–80, Oct. 2000.

[4] C. L. Hovington, A. McGirr, M. Lepage, and M. T. Berlim, "Repetitive transcranial magnetic stimulation (rTMS) for treating major depression and schizophrenia: A systematic review of recent meta-analyses," *Ann. Med.*, vol. 45, no. 4, pp. 308–321, Jun. 2013.

[5] G. Bonmassar, S. W. Lee, D. K. Freeman, M. Polasek, S. I. Fried, and J. T. Gale, "Microscopic magnetic stimulation of neural tissue," *Nature Commun.*, vol. 3, no. 1, p. 921, Jun. 2012.

[6] Z. He, N. Selvamurugan, J. Warshaw, and N. C. Partridge, "Pulsed electromagnetic fields inhibit human osteoclast formation and gene expression via osteoblasts," *Bone*, vol. 106, pp. 194–203, Jan. 2018.

[7] J. Tong *et al.*, "Pulsed electromagnetic fields promote the proliferation and differentiation of osteoblasts by reinforcing intracellular calcium transients," *Bioelectromagnetics*, vol. 38, no. 7, pp. 541–549, Oct. 2017.

[8] J. Kenkre and J. Bassett, "The bone remodelling cycle," *Ann. Clin. Biochem., Int. J. Lab. Med.*, vol. 55, no. 3, pp. 308–327, May 2018.

[9] A. G. Robling and C. H. Turner, "Mechanical signaling for bone modeling and remodeling," *Crit. Rev. Eukaryotic Gene Expression*, vol. 19, no. 4, pp. 319–338, 2009.

[10] F. Bistolfi, "Evidence of interlinks between bioelectromagnetics and biomechanics: From biophysics to medical physics," *Phys. Medica*, vol. 22, no. 3, pp. 71–95, Jul. 2006.

[11] K. P. Esselle and M. A. Stuchly, "Neural stimulation with magnetic fields: Analysis of induced electric fields," *IEEE Trans. Biomed. Eng.*, vol. 39, no. 7, pp. 693–700, Jul. 1992.

[12] T. Pashut *et al.*, "Mechanisms of magnetic stimulation of central nervous system neurons," *PLoS Comput. Biol.*, vol. 7, no. 3, Mar. 2011, Art. no. e1002022.
[13] K. S. Thorne and R. D. Blandford, "Random processes," in *Modern Classical Physics: Optics, Fluids, Plasmas, Elasticticity, Relativity, and Statistical Physics*. Princeton, NJ, USA: Princeton Univ. Press, 2017, ch. 6, p. 313.
[14] J. R. Melcher, *Continuum Electromechanics*. Cambridge, MA, USA: MIT Press, 1981.
[15] K. S. Thorne and R. D. Blandford, "Magnetohydrodynamcs," in *Modern Classical Physics: Optics, Fluids, Plasmas, Elasticticity, Relativity, and Statistical Physics*. Princeton, NJ: Princeton Univ. Press, 2017, ch. 19, p. 313.
[16] C. Androjna *et al.*, "A comparison of alendronate to varying magnitude PEMF in mitigating bone loss and altering bone remodeling in skeletally mature osteoporotic rats," *Bone*, vol. 143, Feb. 2021, Art. no. 115761.
[17] R. J. Midura *et al.*, "Pulsed electromagnetic field treatments enhance the healing of fibular osteotomies," *J. Orthopaedic Res.*, vol. 23, pp. 1035–1046, Sep. 2005.
[18] M. Zborowski, C. Androjna, E. I. Waldorff, and R. J. Midura, "Comparison of therapeutic magnetic stimulation with electric stimulation of spinal column vertebrae," *IEEE Trans. Magn.*, vol. 51, no. 12, pp. 1–9, Dec. 2015.
[19] J. A. Hopkins and F. W. Wehrli, "Magnetic susceptibility measurement of insoluble solids by NMR: Magnetic susceptibility of bone," *Magn. Reson. Med.*, vol. 37, pp. 494–500, Apr. 1997.
[20] J. Akiyama *et al.*, "Formation of c-axis aligned polycrystal hydroxyapatite using a high magnetic field with mechanical sample rotation," *J. Jpn. Inst. Met.*, vol. 70, no. 5, pp. 412–414, 2006.
[21] Y. Xu and B. He, "Magnetoacoustic tomography with magnetic induction (MAT-MI)," *Phys. Med. Biol.*, vol. 50, pp. 5175–5187, Nov. 2005.
[22] L. Zhou, S. Zhu, and B. He, "A reconstruction algorithm of magnetoacoustic tomography with magnetic induction for an acoustically inhomogeneous tissue," *IEEE Trans. Biomed. Eng.*, vol. 61, no. 6, pp. 1739–1746, Jun. 2014.
[23] P. Grasland-Mongrain, E. Miller-Jolicoeur, A. Tang, S. Catheline, and G. Cloutier, "Contactless remote induction of shear waves in soft tissues using a transcranial magnetic stimulation device," *Phys. Med. Biol.*, vol. 61, no. 6, p. 2582, 2016.
[24] M. Honrath and A. Sabouni, "Study of intracranial pressure in human brain during transcranial magnetic stimulation," in *Proc. 37th Annu. Int. Conf. IEEE Eng. Med. Biol. Soc. (EMBC)*, Aug. 2015, pp. 6920–6923.
[25] L. R. Moore *et al.*, "Mechanical resonator to measure magnetic susceptibility of structurally intact bone," *J. Magn. Magn. Mater.*, vol. 521, Mar. 2021, Art. no. 167488.
[26] S. Sammet, "Magnetic resonance safety," *Abdominal Radiol.*, vol. 41, pp. 444–451, Mar. 2016.
[27] C. T. Rubin, H. J. Donahue, J. E. Rubin, and K. J. McLeod, "Optimization of electric field parameters for the control of bone remodeling: Exploitation of an indigenous mechanism for the prevention of osteopenia," *J. Bone Mineral Res.*, vol. 8, no. S2, pp. S573–S581, Dec. 2009.
[28] S. D. Cook, S. L. Salkeld, L. P. Patron, J. P. Ryaby, and T. S. Whitecloud, "Low-intensity pulsed ultrasound improves spinal fusion," *Spine J.*, vol. 1, pp. 246–254, Jul./Aug. 2001.
[29] G. ter Haar, "Therapeutic applications of ultrasound," *Prog. Biophys. Mol. Biol.*, vol. 93, pp. 111–129, Jan./Apr. 2007.
[30] V. Mooney, "A randomized double-blind prospective study of the efficacy of pulsed electromagnetic fields for interbody lumbar fusions," *Spine*, vol. 15, pp. 708–712, Jul. 1990.
[31] C. T. Rubin and K. J. McLeod, "Promotion of bony ingrowth by frequency-specific, low-amplitude mechanical strain," in *Clinical Orthopaedics and Related Research*. Philadelphia, PA, USA: J. B. Lippincott & Co., Jan. 1994, pp. 165–174.
[32] T. L. Smith, D. Wong-Gibbons, and J. Maultsby, "Microcirculatory effects of pulsed electromagnetic fields," *J. Orthopaedic Res.*, vol. 22, pp. 80–84, Jan. 2004.
[33] M. Schnoke and R. J. Midura, "Pulsed electromagnetic fields rapidly modulate intracellular signaling events in osteoblastic cells: Comparison to parathyroid hormone and insulin," *J. Orthopaedic Res.*, vol. 25, no. 7, pp. 933–940, Jul. 2007.
[34] C. A. L. Bassett, R. J. Pawluk, and R. O. Becker, "Effects of electric currents on bone *in vivo*," *Nature*, vol. 204, no. 4959, pp. 652–654, 1964.
[35] R. Goodman, C. A. Bassett, and A. S. Henderson, "Pulsing electromagnetic fields induce cellular transcription," *Science*, vol. 220, no. 4603, pp. 1283–1285, Jun. 1983.
[36] J. Chen and F. Long, "MTOR signaling in skeletal development and disease," *Bone Res.*, vol. 6, no. 1, Dec. 2018.
[37] T. E. Patterson *et al.*, "Exposure of murine cells to pulsed electromagnetic fields rapidly activates the mTOR signaling pathway," *Bioelectromagnetics*, vol. 27, pp. 535–544, Oct. 2006.
[38] A. A. Pilla, "Low-intensity electromagnetic and mechanical modulation of bone growth and repair: Are they equivalent?" *J. Orthopaedic Sci.*, vol. 7, pp. 420–428, May 2002.
[39] Z. Schwartz, M. Fisher, C. H. Lohmann, B. J. Simon, and B. D. Boyan, "Osteoprotegerin (OPG) production by cells in the osteoblast lineage is regulated by pulsed electromagnetic fields in cultures grown on calcium phosphate substrates," *Ann. Biomed. Eng.*, vol. 37, pp. 437–444, Mar. 2009.
[40] J. A. Spadaro, "Mechanical and electrical interactions in bone remodeling," *Bioelectromagnetics*, vol. 18, no. 3, pp. 193–202, 1997.